Theoretical Efficiency and Dosimetry of Buffered On-body Transmitter Antennas for Wireless Powering of In-body Devices

Icaro V. Soares*, Anja K. Skrivervik†, Denys Nikolayev*
*IETR (l'Institut d'électronique et des technologies du numérique) UMR 6164, CNRS / Univ. Rennes, Rennes, France
†Microwaves and Antennas Group, Ecole Polytechnique Federale de Lausanne, Lausanne, Switzerland

***Abstract*—The viable and safe application of wireless power transfer for powering bioelectronic implants requires understanding the wave propagation in heterogeneous and dispersive media, the electromagnetic exposure assessment, and the optimum design of the system parameters to achieve a trade-off between efficiency and specific absorption rate levels. Therefore, based on the case study of a wirelessly charged deep-implanted pacemaker, a parametric analysis on the transmitter dimensions and electromagnetic properties is carried out to achieve such a trade-off. The results show that the system reaches the maximum efficiency without increasing SAR levels when the transmitter is composed of an electric source, an air-like substrate, and a superstrate matched to the wave impedance in the skin with a thickness of half the wavelength in this medium. Furthermore, this configuration is compared to a magnetic counterpart, and the reasons for its suboptimal performance are investigated in terms of near-field, reflection, and attenuation losses.**

***Index Terms*—bioelectronics, efficiency, exposure, implants, pacemakers, wireless power transfer.**

I. Introduction

Bioelectronic implants are being increasingly widespread in medicine, and their applications range from biotelemetry [1], over electroceuticals [2], to high-performance sports medicine [3]. This vast usage range is due to the fact that these devices allow more robust diagnostics, more effective treatments, and more precise monitoring than their counterpart methods traditionally employed. Not to mention that bioelectronic implants are generally much less invasive. However, one major constraint to the further development of these devices is the batteries that occupy most of the volume, limit the power budget, and require frequent maintenance and replacement.

Therefore, to mitigate these limitations and expand the capabilities of these implants, several Wireless Power Transfer (WPT) techniques have been investigated and applied in this context. For instance, it has been shown that inductive coupling methods are particularly efficient for subcutaneous devices such as spinal cord stimulators [4], ocular [5], and cochlear implants [6]. On the other hand, farfield WPT techniques can be used to feed the ultra-low-power sensors used for biotelemetry [7]. In between, mid-field WPT is much more efficient than farfield methods and reach larger distances than inductive coupling. Mid-field WPT is especially advantageous for deep-implanted devices such as pacemakers [8], [9], and brain stimulators [10].

Primary concern about the application of WPT to charging in-body devices is the electromagnetic exposure levels and the user's safety. The Specific Absorption Rate (SAR) regulations restrict the transmitted power levels and require a careful exposure assessment. At the same time, the heterogeneity and dielectric dispersion of the tissues strongly affect the efficiency. Therefore, modeling the electromagnetic wave propagation in the body is essential to understand the loss mechanisms and to obtain a best trade-off between the efficiency and exposure level. For this intent, different approaches have been proposed, such as the semi-analytical spherical harmonics expansion [11], 2D-axisymmetrical full-wave analysis [12], [13], and even more realistic model as presented in [14], [15]. Each of these models presents its advantages and drawbacks, but they agree on the overall behavior of in-body WPT systems and the optimal operating frequency range.

Apart from that, the knowledge of propagation in biological media can be exploited to improve the performance of biomedical devices. In this paper, we propose an on-body transmitter configuration for a deep-implanted pacemaker charging application in which the source is separated from the skin surface by a dielectric superstrate (buffer), which function is to reduce the near-field losses, thus increasing the efficiency and simultaneously reducing the user exposure levels. Then, this paper aims to perform a study of the superstrate's relative electric permittivity and its thickness, i.e., the distance between the source and the skin, in order to achieve the maximum efficiency and minimum exposure.

To achieve this main goal, the problem is physically and mathematically formulated based on an anatomical human pectoral 2D model that is used to derive the wireless power transfer efficiency and peak SAR. Then, a parametric analysis on the buffer is carried out, and, from the obtained results, it is possible to establish the rules of thumb for the design of on-body transmitters in implanted wireless power transfer applications.

II. Problem Formulation

In order to model the wireless charging of a deep-implanted pacemaker, we consider a two-dimensional cross-section of the human pectoral represented in Fig. 1a composed of nine tissues whose dielectric properties are given by [16] and densities by [17]. The receiver (pacemaker) is represented by

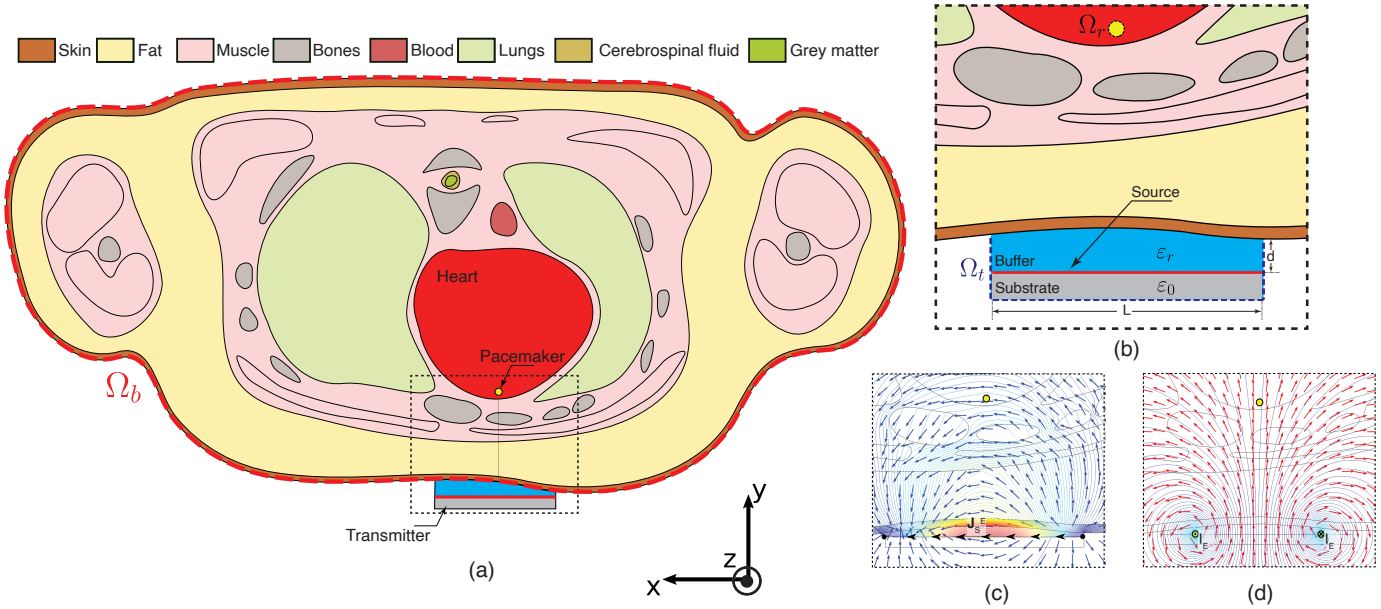

Fig. 1. Formulation for the analyzed problem: (a) 2D model for the human pectoral with nine dispersive tissues. In this model, the transmitter is represented by an on-body source whereas the receiver (pacemaker) is represented by a lossless 1-mm radius circular region matched to the wave impedance at the myocardium at a distance of 37 mm from the skin. (b) Close-up view of the region between the transmitter and receiver. The transmitter is composed by an electric or magnetic source located between a substrate matched to the wave impedance in the free space and a superstrate with electric permittivity ε_r. The regions Ω_t, Ω_r, and Ω_b correspond respectively to the integration domains around the transmitter, the receiver, and the body. (c–d) Electric (blue arrows) and magnetic (red arrows) field distribution for the electric and magnetic source, respectively.

a circular region with a 1 mm radius implanted at the heart, 37 mm from the skin layer, and perfectly aligned to the transmitter outside the body, as proposed in [8]. This receiver is filled with a lossless material perfectly matched to the wave impedance in the heart. The alignment between transmitter and receiver justifies the z-axis invariance, i.e., $\mathbf{E}(x,y,z) = \mathbf{E}(x,y)e^{ik_z z}$, where k_z is the out-of-plane propagation constant and allows us to avoid the high computational cost of simulating the full tridimensional human body model. This assumption is also valid from the point of view of electromagnetic exposure assessment once the highest SAR region is located between the transmitter and receiver. In addition, the high dispersion in the tissues attenuates the field propagation in the z-direction. The transmitter with length $L = 60$ mm ($\sim \lambda/2$ at 2.45 GHz in free space) and external to the body, as shown in Fig. 1b, is composed of a source that can be either electric or magnetic, an air-substrate, and a lossless superstrate with relative permittivity ε_r which separates the source from the skin surface by a distance d. The electric source in Fig. 1c is modeled by a surface current distribution $\mathbf{J}_S^E(x,y,z)$ given by:

$$\mathbf{J}_S^E = \left[\cos\left(\frac{\pi x}{L}\right), 0, 0\right], \tag{1}$$

whereas the magnetic source is represented by two unitary out-of-plane currents IE on the edges of the source and with opposite phases, as illustrated in Fig. 1d. In this way, these sources represent respectively a half-wave dipole and a loop antenna, which is confirmed by the field distribution in Fig. Fig. 1c and Fig. 1d.

Once the physical problem is established, the numerical formulation is proposed. First, the time-harmonic total electric $\mathbf{E}$ and magnetic fields $\mathbf{H}$ are obtained by performing the full-wave 2D simulation in COMSOL Multiphysics®. Then, from energy conservation, the transmitted power P_t is the sum of the received power P_r, dissipated power P_d, and the time-averaged energies stored in the magnetic ($\overline{W_m}$) and electric fields ($\overline{W_e}$) [18]:

$$P_t = P_r + P_d + i2\omega\left(\overline{W_m} - \overline{W_e}\right). \tag{2}$$

The transmitted and received power can be calculated by integrating the power flow over the surface of the transmitter Ω_t and the receiver Ω_r, respectively [14]:

$$P_t = \oint_{\Omega_t}\left(\frac{1}{2}\mathbf{E}\times\mathbf{H}^*\right)\cdot\mathbf{ds}, \tag{3a}$$

$$P_r = \oint_{\Omega_r}\left(\frac{1}{2}\mathbf{E}\times\mathbf{H}^*\right)\cdot\mathbf{ds}. \tag{3b}$$

In this way, the wireless power transfer efficiency η is given by [12]:

$$\eta \equiv \frac{\Re(P_r)}{\Re(P_t)}. \tag{4}$$

For the purposes of dosimetry analysis, it is also essential to calculate the normalized peak specific absorption rate ($\widehat{pSAR}$) as the maximum SAR evaluated over the entire pectoral cross-section surface Ω_b normalized by the transmitted power P_t:

$$\widehat{pSAR} \equiv \max_{\Omega_b}\left(\frac{\sigma\left|\mathbf{E}\right|^2}{\rho}\right)\cdot\frac{1}{P_t}, \tag{5}$$

where σ is the tissue's electric conductivity and ρ its mass density.

III. Analysis of the On-body Transmitter

A. Method of Analysis

The aim is to investigate how the transmitter parameters, that is, the nature of the source, the buffer thickness d, and permittivity ε_r, affect the wireless power transfer efficiency as well as the exposure levels. Thus, a parametric analysis was carried out by running the simulation and performing the calculations described in section 0 within the ranges: $0 \leq d \leq 50$ mm and $1 \leq \varepsilon_r \leq 80$. This last range goes from the free space to approximately the skin permittivity at the analyzed frequency [16]. To perform this parametric analysis, the frequency was set at 2.45 GHz. As it was shown in previous studies on the theoretical limitations for the wireless charging of in-body devices [13], [15], this frequency is in the optimum frequency range ($\approx 0.7 - 3$ GHz). In addition, it is in the Industrial, Scientific, and Medical (ISM) bands, which makes the results more significant for physically realizable systems. The results for this parametric analysis are shown in Fig. 2a for the electric source and Fig. 2b for the magnetic one.

B. Efficiency as a Function of the Transmitter Parameters

Firstly, the results for the efficiency show that the global maximum is achieved for a buffer thickness of 7 mm in the case of an electric source and 6 mm for the magnetic one. However, for the electric source, other local maxima are obtained periodically with the buffer thickness. In fact, by considering the wavelength λ at the skin layer, the global maximum occurs at $\lambda/2$ and the local maxima around its multiples. Even though some local maxima can also be verified for the magnetic source, this periodicity is less noticeable as it presents suboptimal performance, with the maximum efficiency almost an order of magnitude lower than its electric counterpart.

C. Maximum Efficiency and Electromagnetic Exposure

The curves in Fig. 3 show the efficiency and the peak SAR normalized by the transmitted power as a function of the buffer permittivity with the optimum buffer thickness for both electric and magnetic sources. For the electric source, the efficiency increases with the permittivity until approximately reaching a plateau for $\varepsilon_r \geq 65$. One reason for the maximum efficiency to be obtained at high permittivity is the fact that, in this case, the wave impedance contrast between the buffer and the skin is reduced, thus reducing the reflection losses. In addition, the near-field region decreases as the permittivity increases, also reducing the near-field losses [19]. Therefore, in this case, the losses are mainly due to the attenuation in the dispersive tissues, which is confirmed by the similar behavior between the efficiency and the normalized peak SAR for the electric source, except for $\varepsilon_r \geq 80$ due to the increase of the reflection losses.

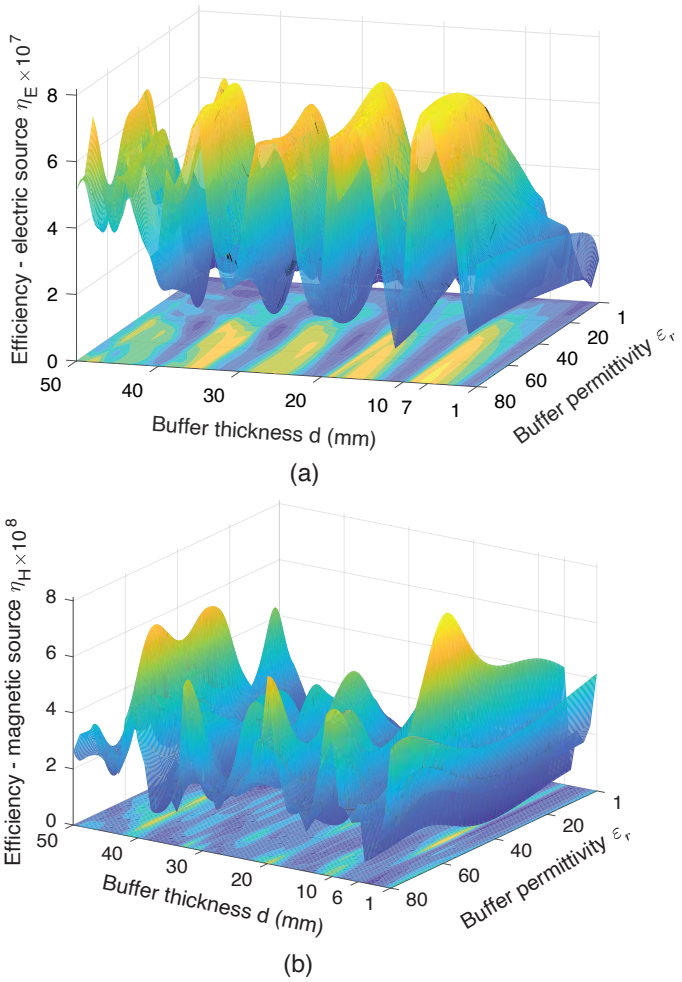

Fig. 2. Wireless power transfer efficiency for the (a) electric and (b) magnetic source as a function of the buffer's thickness d and permittivity ε_r at the frequency of 2.45 GHz

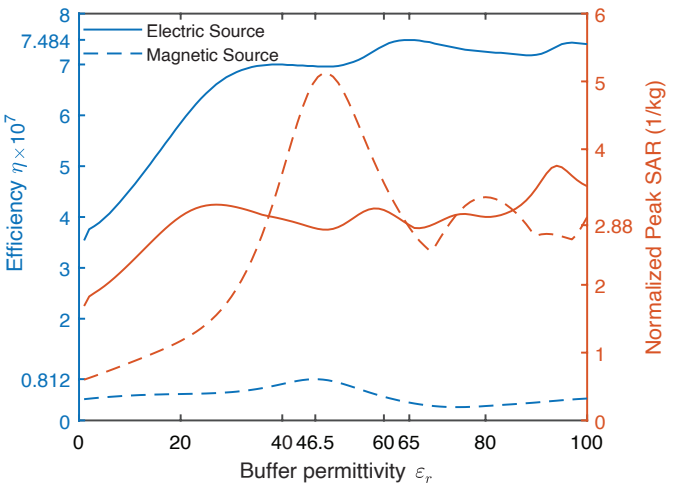

Fig. 3. Efficiency and the peak SAR normalized by the transmitted power as a function of the buffer permittivity for the electric source (continuous line) and magnetic source (dashed line) considering the buffer thickness in which the global maxima are located ($d = 7$ mm for the electric source and $d = 6$ mm for the magnetic source).

As it was also evidenced in Fig. 2b, the magnetic source presents a strongly deteriorated performance, but it reaches its maximum efficiency for $\varepsilon_r = 45.6$, which is also where the maximum SAR levels are verified. The reason for this suboptimal performance is in the fact that in the analyzed case, the magnetic source is not an electrically small antenna and, as the near-field region depends on the antenna size, the near-field is large, and it becomes even larger since the optimum permittivity for this source is lower than the one for the electric source. Therefore, the near-field losses are much higher, which can also be evidenced by the high SAR level for this specific ε_r. Moreover, once there is a significant contrast between the buffer and the skin permittivity, the reflection losses are also more noticeable. Those two losses combined with the attenuation in the tissues lead to a considerable reduction in the power delivered to the receiver and, consequently, a reduction in efficiency.

D. Local SAR Profiles

Finally, the normalized local SAR in the region around the transmitter and receiver is shown for the electric and magnetic source in Fig. 4a and Fig. 4b, respectively. For these graphs, the optimal parameters are considered (electric source: $d = 7$ mm, $\varepsilon_r = 65$; magnetic source: $d = 6$ mm, $\varepsilon_r = 45.6$). Overall, it can be seen that the SAR profile follows the field distribution for both sources, being higher in the center of the half-wave dipole, whereas for the magnetic source, the high SAR region is located around the edges of the loop antenna, similarly as shown in Fig. 1c and Fig. 1d. In addition, as was also revealed in Fig. 3, the maximum SAR level obtained for the magnetic source is almost twice that for the electric source. However, it is mostly concentrated in the skin for the loop antenna, whereas the local SAR in the inner tissues is higher for the dipole antenna. Due to the high near field losses verified for the magnetic source, the power is mostly in the skin layer, while in the electric case, the losses are caused by the attenuation as the wave propagates through the body. Nevertheless, in both cases the SAR levels in the vital organs are negligible.

IV. Conclusion

The application of wireless power transfer techniques for powering implantable bioelectronics has the potential to expand the novel capabilities that these devices have already been bringing to medicine. However, the challenge is to find a trade-off between efficiency and electromagnetic exposure levels to make these wirelessly charged devices viable and safe.

To this intent, an investigation of the influence of on-body transmitter parameters (nature of the source, buffer thickness, and permittivity) on the efficiency and SAR levels is proposed in this paper. In an implantable wireless charging application, the on-body transmitter is the component that presents more degrees of freedom and, thus, is the one that can be most exploited in order to achieve the desired trade-off.

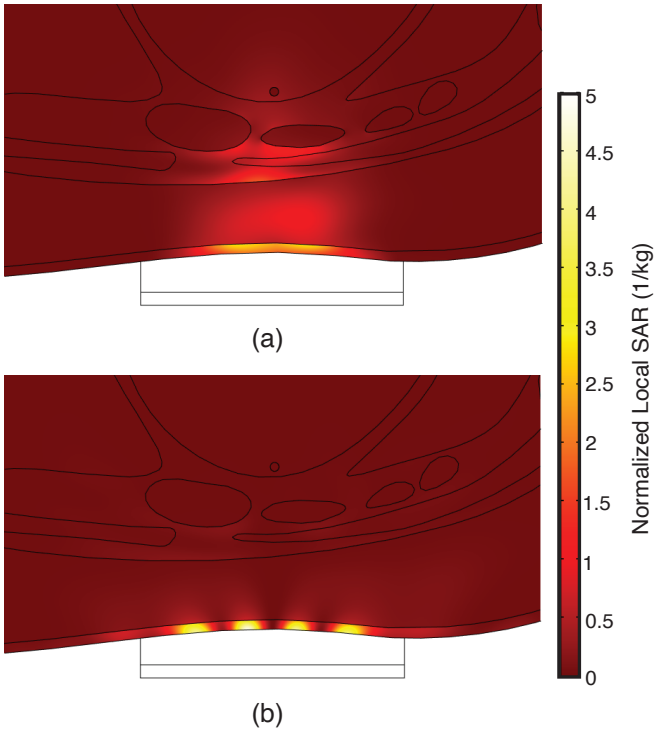

Fig. 4. Surface plot of the local SAR normalized by the transmitted power in the region around the transmitter and receiver for the (a) electric source and (b) magnetic source.

Based on the problem formulated through a realistic human pectoral model, it was verified that for powering a deep-implanted pacemaker, an electric source outperforms a magnetic source, achieving efficiencies almost ten times higher. The maximum efficiency for the electric source is obtained when the buffer permittivity is close to the skin permittivity, and its thickness is around half the wavelength in this medium. This configuration leads to a significant reduction in the reflection and near-field losses, which is not verified for the magnetic source, being it the reason for the suboptimal performance of the latter.

Regarding the electromagnetic exposure levels, the SAR profiles are strongly related to the field produced by both sources and the loss behavior. Once the electric source produces a more intense electric field at its center, and most of the losses are due to the attenuation in the tissues, the peak SAR level is lower than the one verified for the magnetic source, but the local SAR in the inner tissues is higher. However, once most of the power transmitted by the magnetic source is dissipated in the skin layer, the peak SAR is higher and is also located in the skin. Nonetheless, any of the vital organs presented significant local SAR levels.

To sum up, the results presented in this work reveals that for wireless charging deep-implantable bioelectronics, the electric source is the most indicated. In addition, the transmitter's superstrate must be designed so that its permittivity be comparable with the skin permittivity and its thickness around

half the wavelength in this medium. In this way, maximum efficiency can be achieved with low SAR levels.

ACKNOWLEDGMENT

This study was supported by the French region of Brittany through the SAD "EM-NEURO" project No. 227861.

REFERENCES

[1] M. P. Soares dos Santos et al., "Towards an effective sensing technology to monitor micro-scale interface loosening of bioelectronic implants," *Sci. Rep.*, vol. 11, no. 1, p. 3449, Dec. 2021

[2] Y. Long, J. Li, F. Yang, J. Wang, and X. Wang, "Wearable and implantable electroceuticals for therapeutic electrostimulations," *Adv. Sci.*, vol. 8, no. 8, p. 2004023, 2021.

[3] T. Yang et al., "Hierarchically microstructure-bioinspired flexible piezoresistive bioelectronics," *ACS Nano*, vol. 15, no. 7, pp. 11555–11563, Jul. 2021.

[4] F. T. Alrashdan, J. C. Chen, A. Singer, B. W. Avants, K. Yang, and J. T. Robinson,"Wearable wireless power systems for 'ME-BIT' magnetoelectric-powered bio implants," *J. Neural Eng.*, vol. 18, no. 4, p. 045011, Aug. 2021.

[5] M. Yuan et al., "Electronic contact lens: a platform for wireless health monitoring applications," *Adv. Intell. Syst.*, vol. 2, no. 4, p. 1900190, 2020.

[6] S. Hong et al., "Cochlear implant wireless power transfer system design for high efficiency and link gain stability using a proposed stagger tuning method," in *Proc. 2020 IEEE Wireless Power Transfer Conference (WPTC)*, Nov. 2020, pp. 26–29.

[7] A. Iqbal, M. Al-Hasan, I. B. Mabrouk, A. Basir, M. Nedil, and H. Yoo, "Biotelemetry and wireless powering of biomedical implants using a rectifier integrated self-diplexing implantable antenna," *IEEE Trans. Microw. Theory Tech.*, vol. 69, no. 7, pp. 3438–3451, Jul. 2021.

[8] J. S. Ho et al.,"Wireless power transfer to deep-tissue microimplants," *Proc. Natl. Acad. Sci.*, vol. 111, no. 22, pp. 7974–7979, Jun. 2014.

[9] H. Le-Huu and C. Seo, "Bipolar spiral midfield wireless power transfer for cardiac implants application," *IEEE Antennas Wirel. Propag. Lett.*, pp. 1–1, 2021.

[10] Y. Tanabe et al., "High-performance wireless powering for peripheral nerve neuromodulation systems," *PLOS ONE*, vol. 12, no. 10, p. e0186698, Oct. 2017.

[11] M. Gao, D. Nikolayev, M. Bosiljevac, Z. Sipus, and A. K. Skrivervik, "Rules of thumb to assess losses of implanted antennas," in *Proc. 2021 15th European Conference on Antennas and Propagation (EuCAP)*, Mar. 2021, pp. 1–5.

[12] D. Nikolayev, W. Joseph, M. Zhadobov, R. Sauleau, and L. Martens, "Optimal radiation of body-implanted capsules," *Phys. Rev. Lett.*, vol. 122, no. 10, p. 108101, Mar. 2019.

[13] I. V. Soares et al., "'Physical bounds on implant powering efficiency using body-conformal WPT systems," in *Proc. 2020 IEEE Wireless Power Transfer Conference (WPTC)*, Jun. 2021, pp. 1–4.

[14] D. Nikolayev, M. Zhadobov, P. Karban, and R. Sauleau, "Electromagnetic radiation efficiency of body-implanted devices," *Phys. Rev. Appl.*, vol. 9, no. 2, p. 024033, Feb. 2018.

[15] I. V. Soares, R. Sauleau, D. Nikolayev, "Theoretical analysis of electromagnetic exposure to wireless charging systems for deep-body implantable devices," in *Proc. BioEM 2021*, Sep. 2021, pp. 1–5.

[16] S. Gabriel, R. W. Lau, and C. Gabriel, "The dielectric properties of biological tissues: III. Parametric models for the dielectric spectrum of tissues," *Phys. Med. Biol.*, vol. 41, no. 11, pp. 2271–2293, Nov. 1996.

[17] R. L. Mcintosh and V. Anderson, "A comprehensive tissue properties database provided for the thermal assessment of a human at rest," *Biophys. Rev. Lett.*, vol. 05, no. 03, pp. 129–151, Sep. 2010.

[18] J. D. Jackson, *Classical electrodynamics*, 3rd ed. New York: Wiley, 1999.

[19] A. K. Skrivervik, M. Bosiljevac, and Z. Sipus, "Fundamental limits for implanted antennas: maximum power density reaching free space," *IEEE Trans. Antennas Propag.*, vol. 67, no. 8, pp. 4978–4988, Aug. 2019.